PROCEEDINGS A

rspa.royalsocietypublishing.org

Research

Check for updates

Article submitted to journal

Subject Areas:
Non-Hermitian Physics, Topological matter

Keywords:
Non-Hermitian skin effect, topological phases, wave self-healing

Author for correspondence:
Stefano Longhi
e-mail: stefano.longhi@polimi.it

Selective and tunable excitation of topological non-Hermitian quasi-edge modes

Stefano Longhi[1,2]

[1] Dipartimento di Fisica, Politecnico di Milano, Piazza Leonardo da Vinci 32, I-20133 Milano (Italy)
[2] IFISC (UIB-CSIC), Instituto de Fisica Interdisciplinar y Sistemas Complejos, E-07122 Palma de Mallorca (Spain)

Non-Hermitian lattices under semi-infinite boundary conditions sustain an extensive number of exponentially-localized states, dubbed non-Hermitian quasi-edge modes. Quasi-edge states arise rather generally in systems displaying the non-Hermitian skin effect and can be predicted from the nontrivial topology of the energy spectrum under periodic boundary conditions via a bulk-edge correspondence. However, the selective excitation of the system in one among the infinitely-many topological quasi-edge states is challenging both from practical and conceptual viewpoints. In fact, in any realistic system with a finite lattice size most of quasi-edge states collapse and become metastable states. Here we suggest a route toward the selective and tunable excitation of topological quasi-edge states which avoids the collapse problem by emulating semi-infinite lattice boundaries via tailored on-site potentials at the edges of a finite lattice. We illustrate such a strategy by considering a non-Hermitian topological interface obtained by connecting two Hatano-Nelson chains with opposite imaginary gauge fields, which is amenable for a full analytical treatment.

1. Introduction

Non-Hermitian topological physics [1–5] is attracting a considerable interest since the past few years, with a wealth of novel phenomena which do not have any counterpart in corresponding Hermitian topological systems (see [6–48] and references therein).

THE ROYAL SOCIETY PUBLISHING

The ability to experimentally implement and control non-Hermiticity using synthetic lattices has been demonstrated using different physical platforms ranging from photonic [35,38,39,47,48], acoustic [14,45] and micro mechanical [33,34] systems to topolectrical circuits [36,37]. A central result of topological materials is the bulk-edge correspondence: when two materials with different Bloch bulk topological invariants are interfaced, localized edge states emerge with energies that lie within the energy gap of the surrounding bulk media [49,50]. However, such a rather universal result is challenged in non-Hermitian systems, where the bulk-boundary correspondence apparently breaks down [6,10,11] and localization of an extensive number of bulk states at the edges is observed, a phenomenon dubbed the non-Hermitian skin effect [10,11,15]. In general a non-Hermitian lattice possesses two different types of topological edges states: the conventional ones that have a Hermitian counterpart, and the non-Hermitian skin modes without any Hermitian counterpart. This means that two different bulk-boundary correspondences can be established in non-Hermitian topological systems [29]. The former one relates edge states to the wave function bulk topological invariants, however the band topology should be described by the non-Bloch band theory, where the Bloch wave vector is complex and varies over the generalized Brillouin zone [18,19,29]. The latter bulk-boundary correspondence relates edge modes to the spectral topology of the Bloch Hamiltonian over the ordinary Brillouin zone [26,30]. A nontrivial spectral topology, as measured by a non-vanishing winding number W, results in the existence of topological edge modes [1,26,30,42]. Experimental demonstrations of edge states in systems displaying the non-Hermitians skin effect have been reported in recent works [33,35–38]. In particular, localization of the excitation at the interface separating two non-Hermitian lattices with different spectral topological winding numbers has been observed, even in the absence of ordinary edge states, indicating the collapse of all eigenstates at the interface [35,38]. The non-Hermitian skin effect is observable also in bulk systems via the wave packet drift [23].

A general result on bulk-edge correspondence in non-Hermitian systems has been established by considering semi-infinite boundary conditions [1,26]. In non-Hermitian systems under open boundary conditions, the skin edge states provide a complete set of states (a basis) to expand any state in the Hilbert space. The number of skin edge states thus grows linearly with the system size. A somehow different scenario is observed in the (less physical) semi-infinite boundary conditions: in this case an extensive number of *quasi-edge* states, exponentially localized at the single edge of the lattice, are found [1,26], which are topologically characterized by a non-vanishing spectral winding number W [26]. Unlike skin edge states under open boundary conditions, quasi-edge states under semi-infinite boundary conditions provide an over-complete set of states, and contain as a special subset the skin edge states [26]. Clearly, a non-Hermitian system displaying the non-Hermitian skin effect also shows the quasi-edge modes under semi-infinite boundary conditions. Thus, in addition to the bulk signatures [23], the quasi-edge modes provide a signature of the non-Hermitian skin effect. However, a rather challenging and still open question is to find a way to selective excite a single quasi-edge mode, among the infinitely many ones sustained by the system under semi-infinite boundaries. The difficulty is not only practical, due to the complication of realizing semi-infinite boundaries and preparing the system in a pure edge state, but also conceptual. To clarify this point, let us consider as as example a single-band one-dimensional lattice with a nontrivial spectral topology, i.e. with a Bloch Hamiltonian $H(k)$ whose spectrum describes a closed loop in complex energy plane as k spans the ordinary Brillouin zone. A prototypal example is provided by the clean Hatano-Nelson model [1,51], where $H(k)$ describes an ellipse in complex energy plane. According to the bulk-edge correspondence, for any complex energy E internal to the loop with a negative winding number $W(E) < 0$ there exist $|W(E)|$ edge states localized at the left boundary of the lattice under semi-infinite boundary conditions [1,26]. However, as soon as a right boundary is introduced, the edge states collapse and only those with complex energies belonging to the Hamiltonian $H(k)$, with k varying over the generalized Brillouin zone, survive [1]. This result makes the physical relevance of such quasi-edge modes questionable, suggesting that most of them are metastable states that can be observed only transiently for a short time [1].

In this work we show that quasi-edge modes can be selectively and stably excited in a finite-size non-Hermitian lattice from the free dynamical evolution of the system under initial single-site edge excitation, provided that energy at the edges is judiciously supplied to the system. Basically, complex on-site potentials are added at the edges of a finite-size interface, so as to emulate semi-infinite boundary conditions to stabilize a target quasi-edge state. We illustrate this major result by considering quasi-edge modes in the Hatano-Nelson model [1,26,51–53], since it provides the simplest system displaying the non-Hermitian skin effect amenable for a full analytical treatment and accessible to the experiments using synthetic lattices. Specifically, we show selective and tunable excitation of quasi-edge states at the interface (domain wall) between two Hatano-Nelson chains with opposite imaginary gauge fields [46].

2. Quasi-edge modes in the Hatano-Nelson topological interface

The clean Hatano-Nelson model describes the hopping dynamics of a quantum particle on a one dimensional lattice with asymmetry in the left/right hopping amplitudes induced by an imaginary gauge field [1,51,53]. Assuming rather generally an inhomogeneous imaginary gauge field $h = h(n)$, the Schrödinger equation for the wave amplitudes ψ_n at the various lattice sites reads [46]

$$i\frac{d\psi_n}{dt} = \Delta\left\{\exp[h(n+1)]\psi_{n+1} + \exp[-h(n)]\psi_{n-1}\right\} \tag{2.1}$$

where $\Delta\exp(\pm h)$ are the left/right hopping amplitudes.

Let us first briefly recall the topological properties of the Hatano-Nelson model in the homogeneous case $h(n) = h$ constant [1,26]. Under periodic boundary conditions (PBC), with the Ansatz $\psi_n = \exp[ikn - iH(k)t]$ the Hamiltonian in Bloch space reads $H(k) = 2\Delta\cosh(h + ik)$, where $-\pi \le k < \pi$ is the Bloch wave number. The corresponding energy spectrum describes a closed loop (an ellipse) in complex plane [Fig.1(a)], defined by the equation

$$\left(\frac{\mathrm{Re}(H)}{2\Delta\cosh h}\right)^2 + \left(\frac{\mathrm{Im}(H)}{2\Delta\sinh h}\right)^2 = 1. \tag{2.2}$$

The ellipse is travelled clockwise for $h < 0$, and counter-clockwise for $h > 0$. In the bulk of the lattice, a backward (forward) drift current is observed for $h > 0$ ($h < 0$) with a velocity $v = 2\Delta\sinh|h|$ [52]. The spectral topology is described by the winding number $W(E)$ [1,26]

$$W(E) = \frac{1}{2\pi i}\int_{-\pi}^{\pi} dk \frac{d\log\{H(k) - E\}}{dk} \tag{2.3}$$

for a given complex energy E. Clearly, one has $W(E) = 0$ when E is external to the ellipse, while $W(E) = h/|h| = \pm 1$ when E is internal to the ellipse. A bulk-edge correspondence can be established for the edge modes under the semi-infinite boundary conditions (SIBC) [1,26]: for any complex energy E, there are exactly $|W(E)|$ edge eigenstates with eigenenergy E, which are exponentially localized at the left edge of the semi-infinite lattice for $W(E) < 0$, or at the right edge of the semi-infinite lattice for $W(E) > 0$. Therefore, under SIBC the continuous set of the quasi-edge eigenstates entirely fills the interior of the ellipse. Under open boundary conditions (OBC), the energy spectrum collapses to the segment $(-\Delta, \Delta)$ on the real axis [Fig.1(a)], and thus only a subset of edge modes on an open line survive [1,26].

Let us now consider the Hatano-Nelson topological interface [46], where two Hatano-Nelson lattices with different values of the imaginary gauge field are connected [Fig.1(b)]. Specifically, we assume equal but opposite values of the gauge fields by letting in Eq.(2.1) $h(n) = -h < 0$ for $n \le 0$ and $h(n) = h > 0$ for $n > 0$. Clearly, for each of the two Hatano-Nelson chains the PBC energy spectrum is described by the same ellipse in complex energy plane [Eq.(2.2)], but the two ellipses are travelled in opposite directions [Fig.1(b)], leading to opposite values of the winding numbers $W_1(E) = -W_2(E) = 1$ for any energy E in the interior of the ellipse while $W_1(E) = W_2(E) = 0$ for any energy E in the exterior of the ellipse. According to the bulk-boundary correspondence, exponentially-localized topological interface modes do exist at the

interface, for infinitely-extended chains at both sides, at any energy E in the interior of the ellipse, corresponding to different topological numbers $W_1 \neq W_2$ [46]. The explicit form of the interface modes can be readily obtained and reads

$$\psi_n = \exp(ikn + \mu n - h|n| - iEt) \tag{2.4}$$

where $-\pi \leq k \leq \pi$, $-h < \mu < h$ for localization, and

$$E = 2\Delta \cosh(\mu + ik) \tag{2.5}$$

is the complex energy of the interface mode. As the real parameters k and μ are varied, the

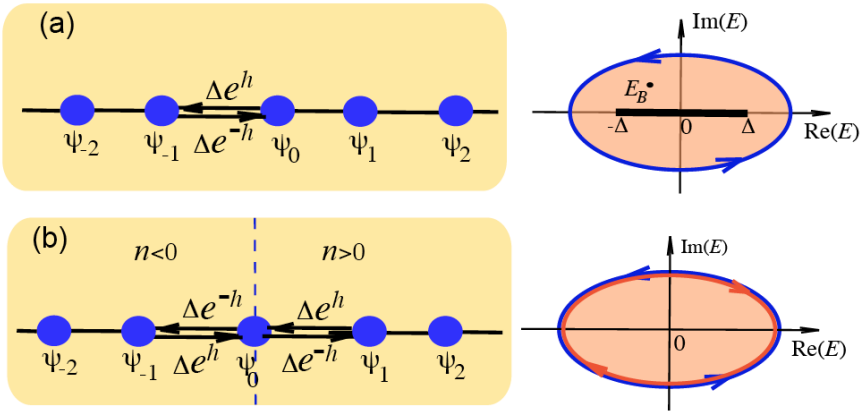

Figure 1. (a) Schematic of the Hatano-Nelson lattice with asymmetric hopping amplitudes $\Delta \exp(\pm h)$. The PBC energy spectrum is an ellipse [Eq.(2.2)] in complex energy plane (right panel), which is traveled clockwise for $h < 0$ and counter-clockwise for $h > 0$. For any complex energy E_B in the interior of the ellipse, the winding number $W(E_B)$ is 1 for $h > 0$ and -1 for $h < 0$, while when E_B lies in the exterior of the ellipse one has $W(E_B) = 0$. According to the bulk-edge correspondence, the interior of the ellipse (shaded area in the figure) corresponds to the energies of quasi-edge states under SIBC. Under OBC, the energy spectrum and corresponding skin modes collapse to the segment $(-\Delta, \Delta)$ on the real energy axis. (b) A topological interface obtained connecting two Hatano-Nelson chains with imaginary gauge fields $-h$ (for $n \leq 0$) and h (for $n > 0$). The right panel shows the two overlapped ellipses, corresponding to the PBC energy spectra of the two bulk lattices, which are traveled in opposite directions. According to the bulk-edge correspondence, interface states do exist for any complex energy E in the interior of the ellipse (shaded area in the figure), where $W_1(E) \neq W_2(E)$.

energies $E = E(k, \mu)$ of the interface modes fill the interior of the ellipse. A main open question arises: is it possible to selectively prepare the system in one of the above topological interface (quasi-edge) modes? This question is not just merely concerning the practical feasibility of exciting the system in the interface mode, rather it regards the true physical relevance of such quasi-edge states [1]. In fact, in a realistic one-dimensional system, such as in a photonic lattice, the number of lattice sites N is always finite and unavoidably open or periodic boundaries usually appear at the edges. Let us consider a finite lattice with sites from $n = -N_1$ to $n = N_2$, with integers $N_{1,2} > 0$ possibly large and $N = N_1 + N_2 + 1$. If we assume, for example, open boundary conditions (i.e. $\psi_n = 0$ for $n > N_2$ and $n < -N_1$), in the thermodynamic limit $N_{1,2} \to \infty$ only a one-dimensional part of the interface states survive, which are picked out from the interface-state continuum, namely the edge states with real energies E on the segment $(-\Delta, \Delta)$, corresponding to $\mu = 0$ and $-\pi \leq k \leq \pi$. All other interface modes thus disappear in a finite-size system, although they can be observed for short times and therefore dubbed *quasi-edge* modes in [1]. Examples of quasi-edge states in a finite-size topological interface will be presented in Sec.4. Here we show that such quasi-edge localized modes can survive, i.e. they can be stabilized, even in finite-sized

systems provided that suitable on-site complex potentials, which supply or take energy from the system, are added at the edges of the chain. The main idea is that the skin edge state (2.4) is an *exact* eigenstate of the Hamiltonian in the finite-size system with open boundary conditions provided that the following on-site potentials are added

$$V_{-N_1} = \Delta \exp(-ik - \mu)\,, \;\; V_{N_2} = \Delta \exp(ik + \mu). \tag{2.6}$$

at the two edges $n = -N_1$ and $n = N_2$ of the lattice. Such complex on-site potentials basically supply energy to the system on one edge (the one with positive imaginary part of the potential, corresponding to gain) and take energy from the system at the other edge (the one with negative imaginary part of the potential, corresponding to loss), effectively emulating an infinitely-extended topological interface. This simple observation suggests one that, after judicious tailoring of the complex on-site potentials at the edges of a finite-size topological interface, it might be possible to stabilize and somehow to selectively excite one among the various edge states of the infinitely-extended interface. The main result of this work, which is proven in the next section, is that the topological interface state (2.4) is obtained from the asymptotic dynamical evolution in the finite-size interface lattice with on-site potentials tailored according to Eq.(2.6), initially excited in the single edge site (either the left or right edge site), provided that $\mathrm{Im}(E) > 0$. This means that, using a finite-size lattice with tailored complex potentials at the two edges, we can selectively excite any one of the topological interface state in the upper half area of the ellipse of Fig.1(b), where $\mathrm{Im}(E) > 0$, but not the topological edge states with energies in the lower half area.

3. Selective excitation of topological interface modes

Let us consider a finite-size Hatano-Nelson topological interface with open boundary conditions, extended from $n = -N_1$ to $n = N_2$, comprising $N = N_1 + N_2 + 1$ sites with the topological interface located at $n = 0$, i.e. with $h(n) = -h < 0$ for $n \leq 0$ and $h(n) = h > 0$ for $n > 0$. We assume that complex on-site potentials V_{-N_1} and V_{N_2}, defined by Eq.(2.6), are added at the two edges of the lattice at sites $n = -N_1$ and $n = N_2$, respectively. The evolution equations of the amplitudes $\psi_n(t)$ in the finite lattice then read

$$i\frac{d\psi_n}{dt} = \Delta\left\{\exp[h(n+1)]\psi_{n+1} + \exp[-h(n)]\psi_{n-1}\right\} + (V_{-N_1}\delta_{n,-N_1} + V_{N_2}\delta_{n,N_2})\psi_n(t) \tag{3.1}$$

($n = -N_1, -N_1+1, ..., 0, 1, ..., N_2$) with the open boundary conditions $\psi_n(t) = 0$ for $n < -N_1$ and $n > N_2$. Without loss of generality, we can assume $\mu < 0$, i.e. $|V_{-N_1}| > \Delta$ and $|V_{N_2}| < \Delta$, as the other case $\mu \geq 0$ is simply obtained by reversing left and right edges of the lattice. The central result of this work is provided by the following:

Theorem. Let us indicate by $\psi_n(t)$ the evolution of the probability amplitudes in the finite-size lattice [Eq.(3.1)] with the initial condition

$$\psi_n(0) = \delta_{n,-N_1}\,, \tag{3.2}$$

corresponding to the excitation of the left edge site of the lattice. Then $\psi_n(t)$ asymptotically evolves toward the topological interface mode (2.4), i.e. $\psi_n(t) \sim \exp(ikn + \mu n - h|n| - iEt)$ as $t \to \infty$, provided that $-h < \mu < 0$ and $\mathrm{Im}(E) > 0$, where $E = 2\Delta\cosh(\mu + ik)$ is the complex energy of the topological skin mode.

In order to prove the above theorem, it is worth first introducing the non-unitary gauge transformation

$$\psi_n(t) = \begin{cases} c_n(t) & n \leq 0 \\ c_n(t)\exp(-2hn) & n \geq 0 \end{cases} \tag{3.3}$$

and to rescale the time variable t so as $\Delta = 1$. The non-unitary gauge transformation (3.3) basically eliminates the topological interface, making the imaginary gauge field uniform all along the finite-size lattice. In fact, under the transformation (3.3) and with $\Delta = 1$ the wave amplitudes $c_n(t)$

satisfy the following coupled equations

$$i\frac{dc_n}{dt} = \exp(-h)c_{n+1} + \exp(h)c_{n-1} + (V_{-N_1}\delta_{n,-N_1} + V_{N_2}\delta_{n,N_2})c_n \tag{3.4}$$

$(n = -N_1, -N_1+1, ..., 0, 1, ...N_2)$ with the open boundary conditions $c_n(t) = 0$ for $n < -N_1$, $n > N_2$ and with the initial condition

$$c_n(0) = \delta_{n,-N_1}. \tag{3.5}$$

Note that, after the gauge transformation (3.3), the interface state (2.4) takes the form

$$c_n^{(skin)}(t) = A\exp[(ik + \mu + h)(n + N_1) - iEt] \tag{3.6}$$

so that to prove the theorem we need to show that

$$\lim_{t\to\infty} \epsilon(t) = 0 \tag{3.7}$$

for a suitable amplitude A, where $\epsilon(t)$ is the deviation function defined by

$$\epsilon(t) \equiv \frac{\|c_n(t) - c_n^{(skin)}(t)\|^2}{\|c_n^{(skin)}(t)\|^2} = \frac{\sum_{n=-N_1}^{N_2} |c_n(t) - c_n^{(skin)}(t)|^2}{\sum_{n=-N_1}^{N_2} |c_n^{(skin)}(t)|^2}. \tag{3.8}$$

The analytical solution $c_n(t)$ to Eqs.(3.4) with the initial condition (3.5) can be obtained using the Laplace transform method (see, for instance, [54]). After introduction of the Laplace transform $\hat{c}_n(s)$ of the wave amplitude $c_n(t)$

$$\hat{c}_n(s) = \int_0^\infty dt c_n(t)\exp(-st) \tag{3.9}$$

with $\mathrm{Re}(s) > \eta > 0$, from Eqs.(3.4) and (3.5) one obtains

$$(is - V_{-N_1}\delta_{n,-N_1} - V_{N_2}\delta_{n,N_2})\hat{c}_n(s) - t_1\hat{c}_{n+1}(s) - t_2\hat{c}_{n-1(s)} = i\delta_{n,-N_1} \tag{3.10}$$

where we have set

$$t_1 \equiv \exp(-h)\,, \quad t_2 \equiv \exp(h). \tag{3.11}$$

Equation (3.10) is a linear algebraic system, that can be solved for $\hat{c}_n(s)$ $(-N_1 \le n \le N_2)$ by the Cramer's rule. As shown below, for our purposes it is enough to calculate $\hat{c}_{-N_1}(s)$, which takes the form

$$\hat{c}_{-N_1}(s) = \frac{i}{is - V_{-N_1} - \Sigma_N(s)} \tag{3.12}$$

where the self-energy $\Sigma_N(s)$ is derived in Appendix A and reads

$$\Sigma_N(s) = \frac{(is - V_{N_2})\sin[(N-1)\theta] - \sin[(N-2)\theta]}{(is - V_{N_2})\sin(N\theta) - \sin[(N-1)\theta]}. \tag{3.13}$$

In the above equation, we introduced the complex angle θ via the relation

$$2\cos\theta = is. \tag{3.14}$$

Once $\hat{c}_{-N_1}(s)$ has been found, the corresponding wave amplitude $c_{-N_1}(t)$ is obtained after inversion as a contour integral in complex s plane (Bromwich integral)

$$c_{-N_1}(t) = \frac{1}{2\pi i}\int_{\mathrm{B}} ds\ \exp(st)\hat{c}_{-N_1}(s) \tag{3.15}$$

where the Bromwich path B is the horizontal contour $\mathrm{Re}(s) = \eta$ in the complex plane and $\eta > 0$ is chosen so that all singularities of $\hat{c}_n(s)$ are below B (Fig.2).

To calculate the Bromwich integral, let us first consider the $N \to \infty$ limit. Assuming the additional constraint $\mathrm{Im}(\theta) > 0$, the self-energy $\Sigma_N(s)$ converges to the simple function

$$\Sigma_\infty(s) = \exp(i\theta) \tag{3.16}$$

and thus

$$\hat{c}_{-N_1}(s) = \frac{i}{is - V_{-N_1} - \Sigma_\infty(s)} = \frac{i}{\exp(-i\theta) - V_{-N_1}}. \tag{3.17}$$

Note that, owing to the constraint $\mathrm{Im}(\theta) > 0$, the self-energy $\Sigma_\infty(s)$ shows a branch cut on the segment I of the imaginary axis defined by $s = i\omega$, with $-2 \leq \omega \leq 2$ [Fig.2(a)]. From Eqs.(3.14) and (3.17), taking into account that $V_{-N_1} = \exp(-ik - \mu)$ and that $\mu < 0$, it readily follows that $c_{-N_1}(s)$ has a single pole at

$$s = s_p = -iE, \tag{3.18}$$

where $E = 2\cosh(\mu + ik)$. Provided that $\mathrm{Im}(E) > 0$, the pole lies above the branch cut. In this case we can compute the Bromwich integral by deforming the contour B as shown in Fig.2(a), so that one has

$$c_{-N_1}(t) = \frac{1}{2\pi i}\int_{\mathrm{H}} ds\ \exp(st)\hat{c}_{-N_1}(s) + \frac{1}{2\pi i}\int_{\sigma} ds\ \exp(st)\hat{c}_{-N_1}(s) \tag{3.19}$$

where the Hankel path H encircles the branch cut I while σ encircles the pole at $s = s_p$. Since $\mathrm{Re}(s_p) > 0$, the latter contribution to the integral dominates over the first contribution for long times, and can be readily computed from the residue of $\hat{c}_{-N_1}(s)$ at $s = s_p$. This yields

$$c_{-N_1}(t) \sim A\exp(-iEt) \tag{3.20}$$

where

$$A = 1 - \frac{1}{V_{-N_1}^2} \tag{3.21}$$

The Hankel path contribution provides a correction to Eq.(3.20), however it remains bounded as $t \to \infty$ and so it can be neglected after an initial transient. Once we have computed the asymptotic behavior of $c_{-N_1}(t)$ at long times, we can directly calculate the asymptotic form of all other amplitudes $c_n(t)$ from Eqs.(3.4) and (3.20) by an iterative procedure using the relations

$$c_{n+1}(t) = i\exp(h)\frac{dc_n}{dt} - V_{-N_1}\exp(h)c_n(t) \quad (n = -N_1) \tag{3.22}$$

$$c_{n+1}(t) = -\exp(2h)c_{n-1}(t) + i\exp(h)\frac{dc_n}{dt} \quad (n > -N_1) \tag{3.23}$$

This yields

$$c_n(t) \sim A\exp[(ik + \mu + h)(n + N_1) - iEt] \tag{3.24}$$

which is valid in the long time limit. From a comparison of Eqs.(3.6) and (3.24) it then readily follows that $\lim_{t\to\infty} \epsilon(t) = 0$, which proves the theorem in the $N \to \infty$ limit.

In a topological interface with finite N, a similar analysis can be performed. In this case the self-energy $\Sigma_N(s)$ is given by Eq.(3.13) and after some straightforward calculations $\hat{c}_{-N_1}(s)$ takes the form

$$\hat{c}_{-N_1}(s) = \frac{\sin[(N+1)\theta] - V_{N_2}\sin(N\theta)}{(s - s_p)\sin[(N+1)\theta]} \tag{3.25}$$

where s_p is given by Eq.(3.18). Clearly, $\hat{c}_{-N_1}(s)$ shows $(N+1)$ poles: one pole is located exactly at $s = s_p = -iE$, like in the $N \to \infty$ limit, whereas the other N poles are obtained at the angles $\theta_l = l\pi/(N+1)$, i.e. $s_l = -2i\cos\theta_l = -2i\cos[l\pi/(N+1)]$ $(l = 1, 2, 3, .., N)$. Note that such additional poles lie on the segment I of the imaginary axis, and become dense on I as $N \to \infty$. In other words, the branch cut I of $\hat{c}_{-N_1}(s)$ in the $N \to \infty$ limit is replaced for finite N by a dense set of poles on I, as shown in Fig.2(b). The Bromwich integral is then given by the sum of the residues arising from the $(N+1)$ poles. Assuming $\mathrm{Im}(E) > 0$, the dominant pole is the one at $s = s_p = -iE$, and thus after an initial transient the asymptotic form of $c_{-N_1}(t)$ is again given by Eqs.(3.20). Once the

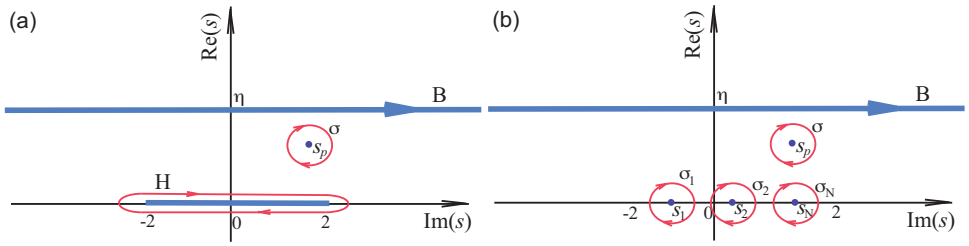

Figure 2. Integration paths in complex s plane used for the calculation of the temporal behavior of the amplitude $c_{-N_1}(t)$ at the left edge site of the topological interface. The horizontal bold line is the Bromwich path B with $\mathrm{Re}(s) = \eta$ and $\eta > 0$ large enough such that all the singularities of $\hat{c}_{-N_1}(s)$ lie below the line B. (a) The case of a topological interface in the $N \to \infty$ limit. In this case $\hat{c}_{-N_1}(s)$ shows a single pole at $s = s_p = -iE$, which lies above the imaginary axis provided that $\mathrm{Im}(E) > 0$, and a branch cut along the segment I on the imaginary axis, from $s = -2i$ to $s = 2i$ (solid bold segment in the figure). The Bromwich path can be deformed to $\sigma \bigcup \mathrm{H}$, where σ encircles the pole $s = s_p$ whereas the Hankel path H encircles the branch cut. (b) The case of a topological interface with a finite number N of lattice sites. In this case $\hat{c}_{-N_1}(s)$ shows $(N+1)$ poles and no branch cuts. The dominant pole is at $s = s_p = -iE$, whereas the other N poles $s_l = -2i\cos[\pi l/(N+1)]$ $(l = 1, 2, 3, ..., N)$ lie on the imaginary axis, between $s = -2i$ and $s = 2i$. The Bromwich path can be deformed to the set of closed loops that encircle the various poles.

asymptotic form of $c_{-N_1}(t)$ has been determined, the asymptotic form of the other amplitudes $c_n(t)$ is obtained from the recursive relations

$$c_{n+1}(t) = i\exp(h)\frac{dc_n}{dt} - V_{-N_1}\exp(h)c_n(t) \quad (n = -N_1) \tag{3.26}$$

$$c_{n+1}(t) = -\exp(2h)c_{n-1}(t) + i\exp(h)\frac{dc_n}{dt} \quad (-N_1 < n \leq N_2 - 1) \tag{3.27}$$

$$\tag{3.28}$$

This yields again the asymptotic form Eq.(3.24) for $c_n(t)$, thus proving the theorem for finite N as well.

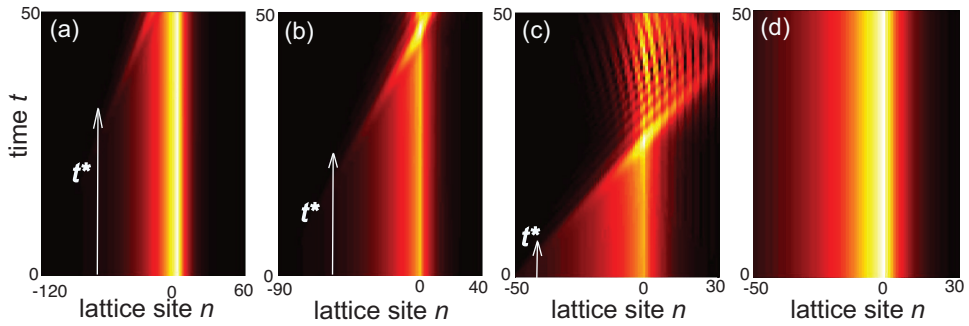

Figure 3. Quasi-edge (metastable) topological interface states in a finite-size Hatano-Nelson interface with open boundary conditions for parameter values $\Delta = 1$ and $h = 0.1$. The system is initially excited in the skin interface state $\psi_n(0) = \exp(ikn + \mu n - h|n|)$ with $\mu = -0.05$ and $k = -\pi/3$. The panels show on a pseudo color map the temporal evolution of the normalized amplitudes $|\psi_n(t)|/\sqrt{\sum_n |\psi_n(t)|^2}$. In (a-c) the edge on-site potentials V_{-N_1} and V_{N_2} vanish, so as the topological skin state survives only for a time t^*, after which it is fully destroyed owing to finite lattice size effects. The time scale t^* increases as the system size $N_{1,2}$ increases [$N_1 = 120, N_2 = 60$ in (a); $N_1 = 90, N_2 = 40$ in (b); $N_1 = 50, N_2 = 30$ in (c)]. As soon as the appropriate potentials $V_{-N_1} = \exp(-ik - \mu)$ and $V_{N_2} = 1/V_{-N_1}$ are added at the left and right edge sites of the lattice, the topological skin state is stabilized, as shown in panel (d).

It should be mentioned that, for a finite value of N, the topological interface state can be dynamically generated for a rather arbitrary initial excitation condition, i.e. not necessarily for a single-site excitation. In fact, in this case the poles of $\hat{c}_{-N_1}(s)$, depicted in Fig.2(b), correspond to the complex eigenenergies of the finite-lattice Hamiltonian of the system. Since the dominant pole, i.e. the pole with the largest imaginary part of the energy, is $s = s_p$, and the interface state is the corresponding eigenvector of the finite-lattice Hamiltonian, it readily follows that after an initial transient the dynamics of the system is attracted toward the interface state, for a rather arbitrary initial excitation of the system.

4. Numerical simulations

We checked the predictions of the theoretical analysis by extended numerical simulations of the coupled equations (3.1) in time domain using an accurate fourth-order variable-step Runge-Kutta method. Some illustrative examples are shown in Figs.3,4 and 5 and 6. In the simulations of Figs.3,4, and 5 we assumed the parameter values $\Delta = 1$, $h = 0.1$, $\mu = -0.05$ and $k = -\pi/3$, corresponding to the eigenenergy $E = 2\Delta\cosh(\mu + ik) = 1.0013 + 0.0866i$ of the interface state and to the on-site potentials $V_{-N_1} = 0.5256 + 0.9104i$, $V_{N_2} = 1/V_{N_1} = 0.4756 - 0.8238i$ at the left and right lattice edges, respectively. Note that, since $\mathrm{Im}(V_{-N_1}) > 0$ (gain) and $\mathrm{Im}(V_{N_2}) < 0$ (loss), energy is basically supplied to the lattice at the left edge site $n = -N_1$, while it is taken from the lattice at the right edge site $n = N_2$. Figures 3(a-c) illustrate the concept of quasi-edge modes [1], i.e. the metastability of the topological interface state in a finite lattice for a few increasing values of $N_{1,2}$ when we set $V_{-N_1} = V_{N_2} = 0$. The results are obtained integrating Eq.(3.1) with $V_{-N_1} = V_{N_2} = 0$ and assuming as an initial condition $\psi_n(t = 0)$ the topological interface state, defined by Eq.(2.4) with truncation at the edges. The figures clearly show that, for $V_{-N_1} = V_{N_2} = 0$ the dynamics looks just like the one of an eigenstate up to some time t^*, above which the state is completely destroyed owing to edge effects. The survival time t^* of the quasi eigenstate increases with the system size $N_{1,2}$, according to the analysis of Ref. [1]. As one can clearly see from Figs.3(a-c), the dominant perturbation that destroys the interface state comes from the cut of the interface mode at the left edge. This is because the localization length of the edge mode is much longer in the $n < 0$ half-space than in the $n > 0$ half-space and $N_1 \sim N_2$. The small perturbation at the left edge introduced by lattice truncation propagates forward, toward the interface, while being amplified owing to the imaginary gauge field h [23,52], until at the time $t \sim t^*$ it reaches the interface region near $n = 0$, destructively interferes with the unperturbed interface state and fully destroys it. At subsequent times, boundary effects arising from the right boundary are also clearly visible [Fig.3(c)]: the initial perturbation reaches the right edge and then propagates backward after being reflected, forming a complex interference pattern. A similar scenario, with the dominant perturbation coming from the right edge of the lattice and propagating backward, would be observed for an interface state with a localization length much longer in the $n > 0$ half-space than in the $n < 0$ half-space. As shown in Fig.3(d), stabilization of the topological interface state is instead observed when we add the appropriate on-site potentials V_{-N_1} and V_{N_2} at the lattice edges, since such additional on-site potentials basically emulate the infinite lattice limit. The most important result provided by the theorem stated in Sec.3 is that the interface state can be dynamically generated by initial single-site excitation of the lattice. This is shown in Fig.4, where the formation and stabilization of the topological interface mode is clearly demonstrated, after an initial time transient, when the on-site potentials V_{-N_1} and V_{N_2} are added at the lattice edges. In particular, according to the theoretical predictions the deviation function $\epsilon(t)$, defined by Eq.(3.8), decays toward zero, indicating the convergence of $\psi_n(t)$ to the topological interface eigenstate $\psi_n^{(skin)}(t)$. As we change the values $V_1 = \exp(-ik - \mu)$ and $V_2 = 1/V_1$ so as to meet the conditions of the main theorem stated in previous section, i.e. $-h < \mu < 0$ and $\mathrm{Im}(E) > 0$, we can selectively generate and tune the dynamically-generated topological interface mode. It should be noted that, since the interface state corresponds to the eigenstate of the finite-lattice Hamiltonian with the highest imaginary part of energy, it can be dynamically excited for a

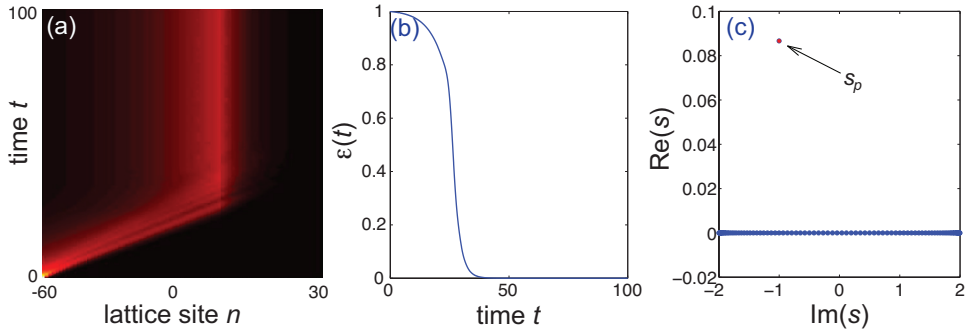

Figure 4. Dynamical formation of the topological interface skin state in a finite Hatano-Nelson lattice with open boundary conditions for parameter values $\Delta = 1$ and $h = 0.1$. The system is initially excited at the left edge site, and on-site potentials $V_{-N_1} = \exp(-ik - \mu)$ and $V_{N_2} = 1/V_{-N_1}$ are added at the left and right edge sites of the lattice ($\mu = -0.05,\ k = -\pi/3$). (a) Temporal evolution on a pseudo color map of the normalized amplitudes $|\psi_n(t)|/\sqrt{\sum_n |\psi_n(t)|^2}$. (b) Behavior of the deviation function $\epsilon(t)$. (c) Poles of $\hat{c}_{-N_1}(s)$ (circles) in the complex s plane. The topological edge mode arises from the dominant pole $s_p = -iE = 0.0866 - 1.0013i$ of $\hat{c}_{-N_1}(s)$.

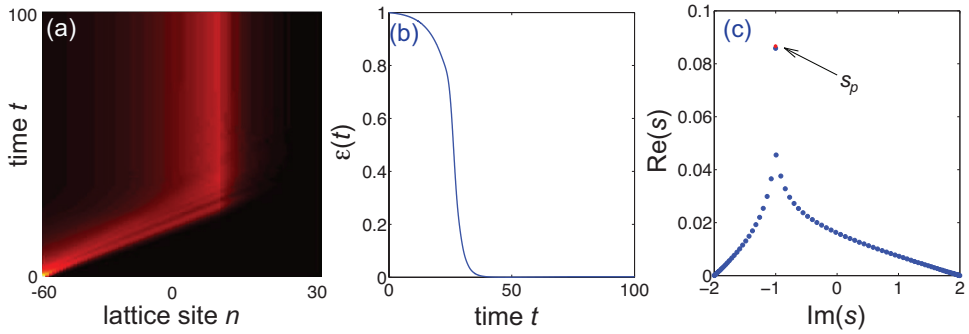

Figure 5. Same as Fig.4, but for $V_{-N_2} = 0$.

rather arbitrary initial excitation of the lattice (not necessarily in a single site). Moreover, in some cases the interface state can be generated even when the on-site potential is added to the left edge site, supplying energy (gain) to the lattice, but not at the right edge, i.e. by assuming $V_{-N_1} = \exp(-ik - \mu)$ and $V_{N_2} = 0$. This is shown in Fig.5. In this case, the location of the $(N + 1)$ poles of the Laplace transform $\hat{c}_{-N_1}(s)$, shown in Fig.5(c), clearly deviates from the distribution predicted by the theoretical analysis [Fig.2(b) and Fig.4(c)]; in particular the dense poles on the imaginary s axis shift toward the $\mathrm{Re}(s) > 0$ half plane, however a dominant pole very close to the theoretical value $s_p = -iE$ survives. This explains why, even though $V_{-N_2} = 0$, the topological interface mode can be dynamically generated after an initial transient, as a result of the dominant pole contribution to $\hat{c}_{-N_1}$. It should be noted that such a result, i.e. excitation of the topological interface mode with only the left on-site complex potential, is very appealing from a practical viewpoint, since it requires just to tune the potential (gain and on-site energy offset) of one site of the lattice. However, this is not possible in all cases, since it requires that the perturbation $V_{N_2} = 0$ does not substantially change the position of dominant poles of $\hat{c}_{-N_1}(s)$. An example is shown in Figs.6 and 7, where in this case stabilization of the topological mode strictly requires both on-site potentials at the two edges.

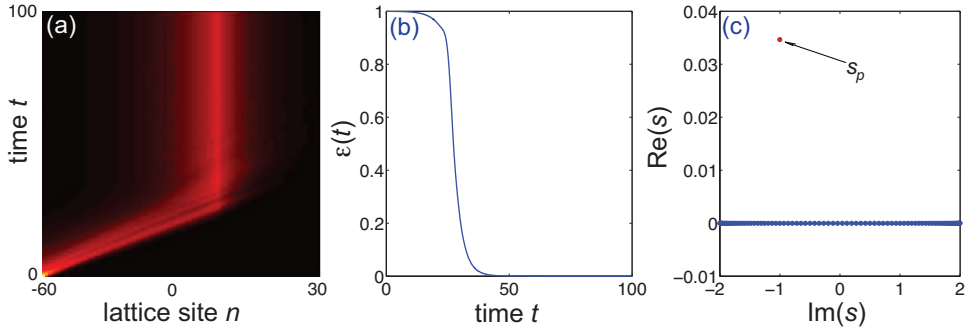

Figure 6. Same as Fig.4, but for $\mu = -0.02$ and $k = -\pi/3$.

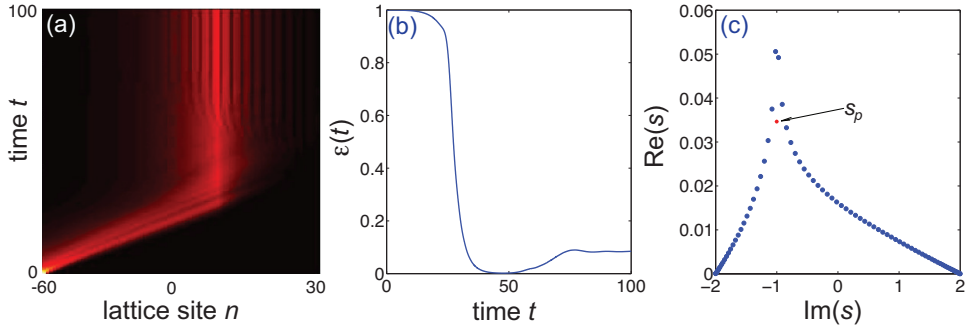

Figure 7. Same as Fig.5, but for $\mu = -0.02$ and $k = -\pi/3$. Note that in this case the vanishing of V_{N_2} largely perturbs the position of poles of $c_{-N_1}(s)$ in the complex s plane, and the topological interface state cannot be dynamically generated. In panel (c) $s_p = -iE$ is the position of the dominant pole predicted by the theoretical analysis in the ideal case $V_{N_2} = 1/V_{-N_1}$.

5. Conclusion

To conclude, in this work we suggested a route toward the selective excitation of topological edge states in a finite-size lattice, based on a judicious tailoring of the complex on-site potentials at the lattice edges. Remarkably, the edge state is dynamically generated by single-site edge excitation of the lattice after an initial transient. Our results indicate that a double-continuum set of quasi-edge states, predicted to exist in semi-infinite non-Hermitian systems displaying the non-Hermitian skin effects, can be stabilized by the edge on-site potentials, preventing their disruption that one would observe in a finite lattice geometry [1]. The method has been illustrated by considering quasi-edge modes at a topological Hatano-Nelson interface, which enables for a full analytical treatment, however the stabilization strategy should be feasible for an extension to other non-Hermitian lattice models: the basic idea is to emulate a semi-infinite geometry in a finite-size lattice by adding suitable complex on-site potentials at the truncated edge. The ability of generating and stabilizing topological quasi-edge states sheds new light onto the physical relevance and robustness of such states, provides a signature of the non-Hermitian skin effect (in addition to the bulk signatures [23]), and could be of potential relevance in future sophisticated applications of non-Hermitian edge modes. For example, topological edge modes in non-Hermitian systems enjoy the fantastic property of being self-healing waves, i.e. the can self-reconstruct their shape after being scattered off by an obstacle [55]. Clearly, to demonstrate and harness such a remarkable property in any application one should be able to stably generate and possibly tune such edge states.

Ethics. There are not ethical issues for this paper.

Data Accessibility. This article has no additional data

Competing Interests. There are not competing interests.

Funding. No fundings for this paper.

Acknowledgements. The author acknowledges the Spanish State Research Agency, through the Severo-Ochoa and Maria de Maeztu Program for Centers and Units of Excellence in R&D (Grant No. MDM-2017-0711).

Disclaimer. No disclaimer for this paper.

A. Derivation of the self-energy

The Laplace transform $\hat{c}_{-N_1}(s)$ of the wave amplitude $c_{-N_1}(t)$ at the edge site $n=-N_1$of the lattice is obtained from the solution of the linear system Eq.(3.10). Using the Cramer's rule, one can write

$$\hat{c}_{-N_1}(s)=\frac{iP_N(s)}{(is-V_{-N_1})P_N(s)-t_1t_2P_{N-1}(s)}=\frac{i}{(is-V_{-N_1})-t_1t_2P_{N-1}(s)/P_N(s)} \tag{A 1}$$

where $P_N(s)$ is $N\times N$ determinant

$$P_N(s)=\begin{vmatrix} is & -t_1 & 0 & 0 & 0 & ... & 0 & 0 & 0 & 0 & 0 \\ -t_2 & is & -t_1 & 0 & 0 & ... & 0 & 0 & 0 & 0 & 0 \\ 0 & -t_2 & is & -t_1 & 0 & ... & 0 & 0 & 0 & 0 & 0 \\ ... & ... & ... & ... & ... & ... & ... & ... & ... & ... & ... \\ 0 & 0 & 0 & 0 & 0 & 0 & ... & -t_2 & is & -t_1 & 0 \\ 0 & 0 & 0 & 0 & 0 & 0 & ... & 0 & -t_2 & is & -t_1 \\ 0 & 0 & 0 & 0 & 0 & 0 & ... & 0 & 0 & -t_2 & is-V_{N_2} \end{vmatrix}. \tag{A 2}$$

Taking into account that $t_1t_2=1$, one obtains

$$\hat{c}_{-N_1}(s)=\frac{i}{is-V_{-N_1}-\Sigma_N(s)} \tag{A 3}$$

where the self-energy is defined by

$$\Sigma_N(s)=\frac{P_{N-1}(s)}{P_N(s)}. \tag{A 4}$$

To calculate the self-energy, we need to compute the determinant $P_N(s)$. Expanding the determinant from the last row, it can be readily shown that

$$P_N(s)=(is-V_{N_2})Q_{N-1}-t_1t_2Q_{N-2}(s) \tag{A 5}$$

where $Q_N(s)$ is the determinant of a $N\times N$ tridiagonal Toeplitz matrix, namely

$$Q_N(s)=\begin{vmatrix} is & -t_1 & 0 & 0 & 0 & ... & 0 & 0 & 0 & 0 & 0 \\ -t_2 & is & -t_1 & 0 & 0 & ... & 0 & 0 & 0 & 0 & 0 \\ 0 & -t_2 & is & -t_1 & 0 & ... & 0 & 0 & 0 & 0 & 0 \\ ... & ... & ... & ... & ... & ... & ... & ... & ... & ... & ... \\ 0 & 0 & 0 & 0 & 0 & 0 & ... & -t_2 & is & -t_1 & 0 \\ 0 & 0 & 0 & 0 & 0 & 0 & ... & 0 & -t_2 & is & -t_1 \\ 0 & 0 & 0 & 0 & 0 & 0 & ... & 0 & 0 & -t_2 & is \end{vmatrix}. \tag{A 6}$$

The determinant $Q_N(s)$ can be readily calculated from the recursive relation $Q_N(s)=isQ_{N-1}(s)-t_1t_2Q_{N-2}(s)$ with $Q_0(s)=1$, $Q_1(s)=is$. Taking into account that $t_1t_2=1$ one

obtains

$$Q_N(s) = \frac{\sin(N+1)\theta}{\sin\theta} \tag{A 7}$$

where we introduced the complex angle θ via the relation

$$2\cos\theta = is. \tag{A 8}$$

Substitution of Eq.(A 7) into Eq.(A 5), one finally obtains the following form of the self-energy $\Sigma_N(s)$ [Eq.(A 4)]

$$\Sigma_N(s) = \frac{(is - V_{N_2})\sin[(N-1)\theta] - \sin[(N-2)\theta]}{(is - V_{N_2})\sin(N\theta) - \sin[(N-1)\theta]}. \tag{A 9}$$

References

1. Gong Z, Ashida Y, Kawabata K, Takasan K, Higashikawa S, Ueda M. 2018 Topological Phases of Non-Hermitian Systems. *Phys. Rev. X* **8**, 031079.
2. Kawabata K, Shiozaki K, Ueda M, Sato M. 2019 Symmetry and Topology in Non-Hermitian. Physics *Phys. Rev. X* **9**, 041015.
3. Ghatak A, Das T. 2019 New topological invariants in non-Hermitian systems. *J. Phys.: Condens. Matter* **31**, 263001.
4. Foa Torres LEF. 2020 Perspective on topological states of non-Hermitian lattices. *J. Phys.: Materials* **3**, 014002.
5. Bergholtz EJ, Budich JC, Kunst FK. 2021 Exceptional Topology in non-Hermitian Systems. *Rev. Mod. Phys.* **93**, 15005.
6. Lee TE. 2016 Anomalous Edge State in a Non-Hermitian Lattice. *Phys. Rev. Lett.* **116**, 133903.
7. Leykam D, Bliokh KY, Huang C, Chong YD, Nori F. 2017 Edge Modes, Degeneracies, and Topological Numbers in Non-Hermitian Systems. *Phys. Rev. Lett.* **118**, 040401.
8. Shen H, Zhen B, Fu L. 2018 Topological Band Theory for Non-Hermitian Hamiltonians. *Phys. Rev. Lett.* **120** 146402.
9. Longhi S. 2018 Non-Hermitian gauged topological laser array, *Annalen der Physik* **530**, 1800023.
10. Kunst FK, Edvardsson E, Budich JC, Bergholtz EJ. 2018 Biorthogonal Bulk-Boundary Correspondence in Non-Hermitian Systems. *Phys. Rev. Lett.* **121**, 026808.
11. Yao S, Wang Z. 2018 Edge States and Topological Invariants of Non-Hermitian Systems. *Phys. Rev. Lett.* **121**, 086803.
12. Martinez Alvarez VM, Barrios Vargas JE, Foa Torres LEF. 2018 Non-Hermitian robust edge states in one dimension: Anomalous localization and eigenspace condensation at exceptional points. *Phys. Rev. B* **97**, 121401(R).
13. Yao S, Song F, Wang Z. 2018 Non-Hermitian Chern Bands. *Phys. Rev. Lett.* **121**, 136802.
14. Zhu W, Fang X, Li D, Sun Y, Li Y, Jing Y, Chen H. 2018 Simultaneous observation of a topological edge state and exceptional point in an open and non-Hermitian acoustic system. *Phys. Rev. Lett.* **121**, 124501.
15. Lee CH, Thomale R. 2019 Anatomy of skin modes and topology in non-Hermitian systems. *Phys. Rev. B* **99**, 201103(R).
16. Liu CH, Jiang H, Chen S. 2019 Topological classification of non-Hermitian systems with reflection symmetry. *Phys. Rev. B* **99** 125103.
17. Edvardsson E, Kunst FK, Bergholtz EJ. 2019 Non-Hermitian extensions of higher-order topological phases and their biorthogonal bulk-boundary correspondence. *Phys. Rev. B* **99**, 081302(R).
18. Song F, Yao S, Wang Z. 2019 Non-Hermitian Topological Invariants in Real Space. *Phys. Rev. Lett.***123**, 246801.
19. Yokomizo K, Murakami S. 2019 Non-Bloch Band Theory for Non-Hermitian Systems. *Phys. Rev. Lett.* **123**, 066404.
20. Jin L, Song Z. 2019 Bulk-Boundary Correspondence in Non-Hermitian Systems in one dimension with chiral inversion symmetry. *Phys. Rev. B* **99**, 081103(R).
21. Liu T, Zhang YR, Ai Q, Gong Z, Kawabata K, Ueda M, Nori F. 2019 Second-order topological phases in non-Hermitian systems. *Phys. Rev. Lett.* **122**, 076801.
22. Herviou L, Bardarson JH, Regnault N. 2019 Defining a bulk-edge correspondence for non-Hermitian Hamiltonians via singular-value decomposition. *Phys. Rev. A* **99**, 052118.

23. Longhi S. 2019 Probing non-Hermitian skin effect and non-Bloch phase transitions. *Phys. Rev. Research* **1**, 023013.
24. Borgnia DS, Kruchkov AJ, Slager RJ. 2020 Non-Hermitian Boundary Modes and Topology. *Phys. Rev. Lett.* **124**, 056802.
25. Lee JY, Ahn J, Zhou H, Vishwanath A. 2019 Topological Correspondence between Hermitian and Non-Hermitian Systems: Anomalous Dynamics. *Phys. Rev. Lett.* **123**, 206404.
26. Okuma N, Kawabata K, Shiozaki K, Sato M. 2020 Topological Origin of Non-Hermitian Skin Effects. *Phys. Rev. Lett.* **124**, 086801.
27. Longhi S. 2019 Topological phase transition in non-Hermitian quasicrystals. *Phys. Rev. Lett.* **122**, 237601.
28. Longhi S. 2020 Non-Bloch-Band Collapse and Chiral Zener Tunneling. *Phys. Rev. Lett.* **124**, 066602.
29. Yang Z, Zhang K, Fang C, Hu J. 2020 Non-Hermitian Bulk-Boundary Correspondence and Auxiliary Generalized Brillouin Zone Theory. *Phys. Rev. Lett.* **125**, 226402.
30. Zhang K, Yang Z, Fang C. 2020 Correspondence between winding numbers and skin modes in non-hermitian systems. *Phys. Rev. Lett.* **125**, 126402.
31. Lee CH, Longhi S. 2020 Ultrafast and anharmonic Rabi oscillations between non-Bloch bands. *Commun. Phys.* **3**, 147.
32. Li L, Lee CH, Mu S, Gong J. 2020 Critical non-Hermitian Skin Effect. *Nature Commun.* **11**, 5491.
33. Ghatak A, Brandenbourger M, van Wezel J, Coulais C. 2020 Observation of non-Hermitian topology and its bulk-edge correspondence. *Proc Nat. Acad. Sci.* **117**, 29561.
34. Gao P, Willatzen M, Christensen J. 2020 Anomalous Topological Edge States in Non-Hermitian Piezophononic Media. *Phys. Rev. Lett.* **125**, 206402.
35. Xiao L, Deng T, Wang K, Zhu G, Wang Z, Yi W, Xue P. 2020 Observation of non-Hermitian bulk-boundary correspondence in quantum dynamics. *Nature Phys.* **16**, 761.
36. Helbig T, Hofmann T, Imhof S, Abdelghany M, Kiessling T, Molenkamp LW, Lee CH, Szameit A, Greiter M, Thomale R. 2020 Generalized bulk-boundary correspondence in non-Hermitian topolectrical circuits. *Nature Phys.* **16**, 747.
37. Hofmann T, Helbig T, Schindler F, Salgo N, Brzezinska M, Greiter M, Kiessling T, Wolf D, Vollhardt A, Kabasi A, Lee CH, Bilusic A, Thomale R, Neupert T 2020. Reciprocal skin effect and its realization in a topolectrical circuit. *Phys. Rev. Research* **2**, 023265.
38. Weidemann S, Kremer M, Helbig T, Hofmann T, Stegmaier A, Greiter M, Thomale R, Szameit A. 2020 Topological funneling of light. *Science* **368**, 311.
39. Song Y, Liu W, Zheng L, Zhang Y, Wang B, Lu P. 2020 Two-dimensional non-Hermitian Skin Effect in a Synthetic Photonic Lattice. *Phys. Rev. Applied* **14**, 064076.
40. Hu H, Zhao E. 2010 Knots and Non-Hermitian Bloch Bands *Phys. Rev. Lett.* **126**, 010401.
41. Zirnstein HG, Refael G, Rosenow B. 2021 Bulk-Boundary Correspondence for Non-Hermitian Hamiltonians via Green Functions. *Phys. Rev. Lett.* **126**, 216407.
42. Wang K, Dutt A, Yang KY, Wojcik CC, Vuckovic J, Fan S. 2021 Generating arbitrary topological windings of a non- Hermitian band. *Science* **371**, 1240.
43. Guo CX, Liu CH, Zhao XM, Liu Y, Chen S. 2021 Exact Solution of Non-Hermitian Systems with Generalized Boundary Conditions: Size-Dependent Boundary Effect and Fragility of the Skin Effect. *Phys. Rev. Lett.* **127**, 116801.
44. Wang K, Dutt A, Wojcik CC, Fan S. 2021 Topological complex-energy braiding of non-Hermitian bands. *Nature* **598**, 59.
45. Zhang X, Tian Y, Jiang JH, Lu MH, Chen YF. 2021 Observation of higher-order non-Hermitian skin effect. *Nat. Commun.* **12**, 5377.
46. Longhi S. 2021 Bulk-edge correspondence and trapping at a non-Hermitian topological interface. *Opt. Lett.* **46**, 6107.
47. Wang K, Li T, Xiao L, Han Y, Yi W, Xue P. 2021 Detecting non-Bloch topological invariants in quantum dynamics. arXiv:2107.14741.
48. Weidemann S, Kremer M, Longhi S, Szameit A. 2022 Topological triple phase transition in non-Hermitian Floquet quasicrystals. *Nature* **601**, 354.
49. Qi XL, Wu YS, Zhang SC. 2006 General theorem relating the bulk topological number to edge states in two-dimensional insulators. *Phys. Rev. B* **74**, 045125.
50. Lu L, Joannopoulos JD, Soljačic M. 2014 Topological Photonics. *Nat. Photon.* **8**, 821.
51. Hatano N, Nelson DR. 1996 Localization Transitions in Non-Hermitian Quantum Mechanics. *Phys. Rev. Lett.* **77**, 570.

52. Longhi S, Gatti D, Della Valle G. 2015 Robust light transport in non-Hermitian photonic lattices. *Sci. Rep.* **5**, 13376.
53. Longhi S, Gatti D, Della Valle G. 2015 Non-Hermitian transparency and one-way transport in low-dimensional lattices by an imaginary gauge field. *Phys. Rev. B* **92**, 094204.
54. Longhi S. 2006 Non-Markovian decay and lasing condition in an optical microcavity coupled to a structured reservoir. *Phys. Rev. A* **74**, 063826.
55. Longhi S. 2021 Self-healing of non-Hermitian topological skin modes (submitted for publication).